Dependence of stimulated Brillouin scattering on target material and *f* number

C. E. Clayton, C. Joshi, A. Yasuda,[a] and F. F. Chen

Department of Electrical Sciences and Engineering, University of California, Los Angeles, California 90024
(Received 24 March 1981; accepted 17 September 1981)

Stimulated Brillouin scattering of CO_2 laser radiation from a pre-ionized gas target is observed and studied with the following parameter changes: (1) $f/7.5$ focusing versus $f/2$ focusing, (2) nitrogen plasma versus hydrogen plasma, (3) pure nitrogen versus nitrogen with a hydrogen impurity, and (4) single line operation of the laser versus multiline operation. The f-number dependence is found to be weak because the increased intensity with the smaller f number is offset by the shorter interaction length for the Brillouin instability. The instability growth in nitrogen is found to be more severe than in hydrogen because the nitrogen plasma has a higher ZT_e/T_i resulting in a lower damping rate for the ion-acoustic wave. In all the above cases the Brillouin reflectivity reaches saturation and the inferred saturation amplitudes of the ion-acoustic waves are consistent with ion trapping being the saturation mechanism. Addition of a small amount ($\simeq 6\%$) of a light ion impurity (hydrogen) to a heavy ion plasma (nitrogen) virtually extinguishes the Brillouin instability. Finally, multiline operation of the CO_2 laser pump, with the line separation $\Delta\omega$ and the instability growth rate γ such that $\Delta\omega/\gamma \gg 1$, is seen to reduce the Brillouin reflectivity as if each line were acting independently, as expected.

I. INTRODUCTION

Although much progress has been made in understanding the physics of stimulated Brillouin scattering[1] in controlled laser-plasma experiments, there still remains some uncertainty in what Brillouin reflectivity to expect from a given set of experimental conditions. Reflectivities have been reported over a very wide ($\simeq 5\%$ to $\simeq 60\%$) range.[2-4] The experimental variables leading to these discrepancies in reflectivities include (1) intensity and wavelength regime, (2) pulse length and shape, (3) target material, (4) initial condition of target, and (5) focusing f number. We have previously reported[5] an example of variable (4) in which the promptness of the Brillouin scattered signal depended on the initial ionization level of the target gas.

We have therefore carried out a detailed parametric study of stimulated Brillouin scattering of CO_2 laser radiation in the intensity range of 5×10^{10}–2.5×10^{12} W cm^{-2} from pre-ionized gas targets. The f-number dependence of Brillouin backscatter is found to be weak because the increased intensity at the smaller f number is offset by the shorter focal length, i.e., shorter interaction length, for the instability. We also find the stimulated Brillouin scattering to be more severe in a nitrogen plasma than in a hydrogen plasma because the nitrogen plasma tends to have a higher ZT_e/T_i and, therefore, reduced Landau damping of the ion acoustic wave. The effect of adding a small amount of hydrogen to the nitrogen plasma is also studied, and we find that the Brillouin scattering is virtually extinguished with an approximately 6% proton impurity. Also, when the CO_2 laser is run on three discrete lines, Brillouin scattering levels are reduced as if the stronger line is acting independent of the two weaker lines.

II. EXPERIMENTAL APPARATUS

The CO_2 laser system supplies approximately 36 J on target, about half of which is in a 50 nsec FWHM pulse giving a peak power of 350 MW. The 10 cm diam beam is focused by either an $f/7.5$ or an $f/2$ germanium lens to vacuum intensities of 5×10^{11} W/cm^2 or 2.5×10^{12} W/cm^2 and measured half-intensity spot diameters of 300 or 130 μm, respectively. Multiline operation is accomplished by inserting an SF_6 cell into the oscillator cavity. Preferentially absorbing the 10.6 μm radiation allows the oscillator to run on the 10.3 and 9.6 μm lines.

The pre-ionization is accomplished by pulsing on an arc discharge slightly before the arrival of the CO_2 laser pulse. The beam is focused radially to the center of the cylindrical, approximately 4-cm-diam, arc discharge plasma (Fig. 1). The filling gas is either 15 Torr of hydrogen or 6 Torr of nitrogen.

Backscattered light is split off with a Mylar beam splitter and sent to two liquid helium cooled photoconducting detectors. One detector is placed behind a piezoelectric-driven Fabre–Perot interferometer, and the other is used to monitor the total frequency integrated backscatter.

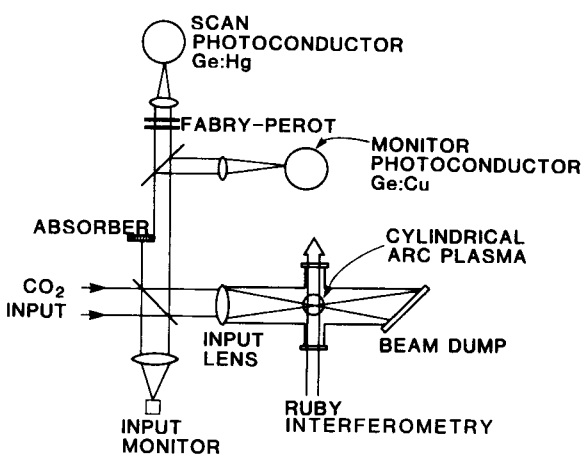

FIG. 1. Schematic of target chamber and backscatter diagnostics. The input lens is either $f/7.5$ or $f/2$, and the fill gas is either hydrogen or nitrogen.

[a]Present address: Department of Navigation Engineering, Tokyo University of Mercantile Marine, Tokyo, Japan.

 0031-9171/81/122312-07$00.90

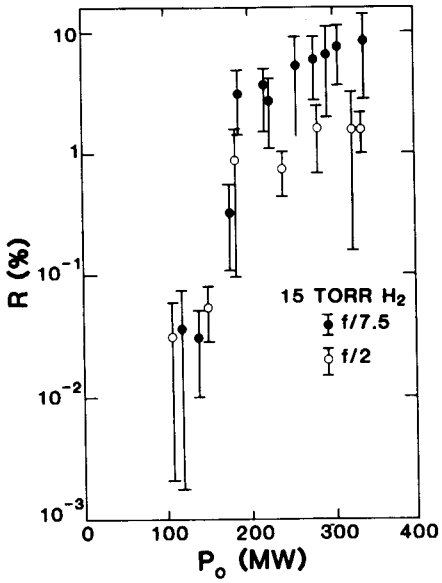

FIG. 2. Brillouin power reflectivity versus input power in a hydrogen plasma for $f/7.5$ focusing (●) and $f/2$ focusing (○).

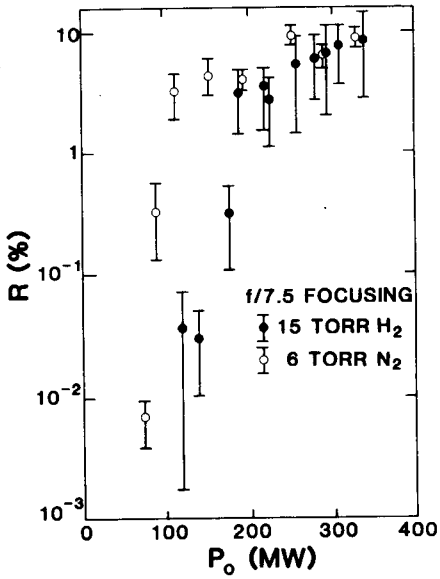

FIG. 3. Brillouin power reflectivity versus input power with $f/7.5$ focusing in hydrogen (●) and nitrogen (○).

The plasma is diagnosed by ruby interferometry along the axis shown in Fig. 1.

III. RESULTS

A. Comparing *f* numbers

The power dependence of the Brillouin reflectivity is shown in Fig. 2 for the $f/7.5$ and $f/2$ focusing optics. In this case, the target was 15 Torr of pre-ionized hydrogen gas. We see that the Brillouin reflectivity grows exponentially with increasing power and then saturates at $P_0 \simeq 190$ MW. Below saturation, the two cases give comparable reflectivities for equal input power even though the intensity in the $f/2$ case is approximately five times higher than in the $f/7.5$ case. The reflectivities begin to saturate at approximately 3% and 0.7% for the $f/7.5$ and $f/2$ cases, respectively. We also note that the reflectivities are not completely saturated but continue to grow slowly with increasing power.

B. Comparing gases

The growth curves for 6 Torr of nitrogen and for 15 Torr of hydrogen using the $f/7.5$ focusing lens are shown together in Fig. 3. As in hydrogen, the Brillouin reflectivity in nitrogen grows exponentially and saturates at approximately 3%. However, the growth is more rapid with increasing power than in hydrogen and the saturation occurs sooner, i.e., at approximately 100 MW as compared with 190 MW in hydrogen. Again, as in hydrogen, the reflectivity shows a slow increase beyond the saturation point.

C. Light ion impurity

Although the saturation levels in pure nitrogen and in pure hydrogen with the $f/7.5$ lens are comparable, when

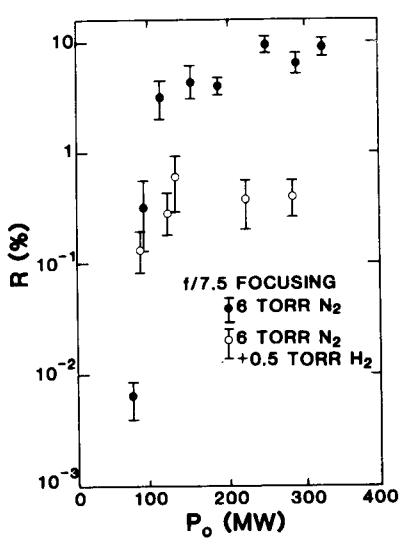

(a)

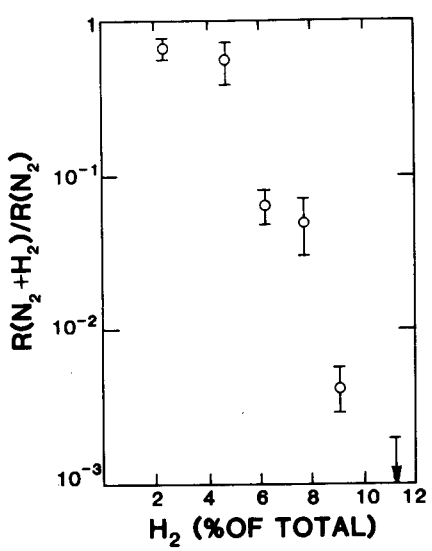

(b)

FIG. 4. Effect of a light ion impurity. (a) Brillouin power reflectivity versus input power with $f/7.5$ focusing in pure nitrogen (●) and in nitrogen plus 8% hydrogen (○). (b) Brillouin power reflectivity at full input power versus concentration of hydrogen added to pure nitrogen. Reflectivities are normalized to the reflectivity in pure nitrogen.

TABLE I. Measured acoustic red shifts of the Brillouin backscatter, measured electron densities, and fill pressures with the various f number and gas combinations.

Gas (f number)	$\Delta\nu$ (GHz)	n_e ($\times 10^{17}$ cm^{-3})	P (Torr)
$H_2(f/7.5)$	11.8	3	15
$H_2(f/2)$	14.0	3	15
$N_2(f/7.5)$	9.5	1	6
$N_2/H_2(f/7.5)$	8.0	1	6/0.5

a small amount (8%) of hydrogen is added to nitrogen, the level of the Brillouin reflectivity is dramatically reduced. This is illustrated in Figs. 4(a) and (b). The curves in Fig. 4(a) show the Brillouin reflectivity from 6 Torr of nitrogen and from 6 Torr of nitrogen plus 0.5 Torr of hydrogen. The saturated reflectivity is reduced by a factor of approximately 10. Figure 4(b) shows how the reflectivity at full input power varies with the percent of hydrogen added to a fixed amount of nitrogen. We see that the stimulated Brillouin scattering is virtually extinguished with a six percent proton impurity.

D. Spectra

In addition to the exponential growth with increasing input power, another signature of stimulated Brillouin scattering is a spectrum red-shifted from the incident CO_2 laser light frequency by $\Delta\nu \simeq 2c_s/\lambda_0$, where c_s is the ion acoustic speed and λ_0 is the incident wavelength. We have assumed k matching for direct backscatter so that the ion acoustic wavelength is $\lambda_0/2$. Indeed, red-shifted backscatter was observed in all the cases presented here, and the shifts are summarized in Table I. In the case of nitrogen plus 8% hydrogen, there are two modes of the ion acoustic wave,[6] however, the spectrum showed no sign of having two peaks.

E. Multiline operation

Multiline operation of the laser can reduce the growth of parametric instabilities such as stimulated Brillouin scattering if the frequency difference between two adjacent lines, $\Delta\omega$, is large compared with the instability growth rate γ (Ref. 7). In this case, each line will act independently, thus effectively reducing the pump strength driving the instability although the total intensity is constant. By introducing an 8 cm long SF_6 cell into the oscillator cavity, we were able to run our laser system on one line, 9.55 μm at 200 MW, or on three lines, 9.55, 10.274, and 10.26 μm with powers 100, 50, and 50 MW, respectively. With three lines, the stimulated Brillouin scattering (nitrogen plasma, $f/7.5$ focusing) was reduced from the one line case by approximately 4.7 ± 2.4 times. This is consistent with the nitrogen growth curve of Fig. 3 if the scatter in the three-line case were due mainly to the 9.55 μm line. The 9.5 μm line is sufficiently far from the 10.3 μm lines so that $\Delta\omega/\gamma \gg 1$ is satisfied.

F. Plasma diagnostics

The main diagnostic used was ruby interferometry along the axis perpendicular to both the incident laser axis and the axis of the arc discharge. Abel inversion of the interferograms gives the plasma density in the interaction region and also its length. Table I summarizes the measured electron densities and fill pressures used with the various f number and gas combinations. The electron and ion temperatures are not measured directly but can be inferred from the experimental data, as will be discussed in the next section.

IV. DISCUSSION

In discussing the results, it is helpful to break up the growth curve into two parts, the exponential growing part and the saturation region. We shall discuss the f number and Z dependence of the growth region first, and the saturation levels second.

A. Dependence on f number

The convective theory of stimulated Brillouin scattering predicts that, for $ZT_e \gg T_i$, the scattered power P_s is given by $P_s = P_n e^N$, where P_n is the noise level from which the scatter grows and N is the exponentiation factor (number of e foldings) given by

$$N = \frac{2\gamma_0^2 L}{c\gamma_i} = \frac{4\pi r_0}{mc^2\omega_0}\frac{\omega_{pi}^2}{\omega_i\gamma_i} I_0 L , \tag{1}$$

where γ_0 is the homogeneous growth rate of stimulated Brillouin scattering, L is the interaction length, γ_i is the damping rate of the ion acoustic wave, $r_0 \equiv e^2/mc^2$ is the classical electron radius, ω_0 is the frequency of the incident laser light, ω_i is the ion acoustic frequency, and I_0 is the incident light intensity.

The convective theory quoted here is based on a steady state; i.e., that Brillouin scatter grows in space but not in time. The theory is not valid for time scales smaller than 10 or 20 growth times. Taking the growth time as γ_0^{-1}, where $\gamma_0^{-1} = 0(10^{-11}\,\text{sec})$ is the usual homogeneous growth rate for stimulated Brillouin scattering, one finds that the minimum time needed to establish a steady state is a few tenths of nanoseconds. The Brillouin scattered signal typically appears in spikes shorter than 5 nsec in width, with detection-bandwidth limited risetimes, and so there is sufficient time for a steady state to develop. We do not know why the scattered signal turns off after approximately an acoustic transit time of a few nanoseconds.

We see from Eq. (1) that for constant plasma parameters the scattered power will vary as $I_0 L$, where L is determined by the shorter of (a) the length of the uniform plasma, or (b) the depth of focus of the beam. For a Gaussian beam, the latter can be expressed as $L = 2\pi w_0^2/\lambda_0$, where w_0 is the spot radius. Since I_0 is $P_0/\pi w_0^2$, so that $I_0 L$ is independent of spot size, the focusing f number, with all else constant, should have little effect on the power scaling of stimulated Brillouin scattering as long as the plasma is longer than the depth of focus.

From the measured intensity and the depth of focus,

we find that I_0L is approximately the same for each lens and is approximately 5×10^{11} W/cm with $L(f/7.5)\simeq 1$ cm and $L(f/2)\simeq 2$ mm. From interferometry we find the plasma to be approximately 3×10^{17} cm^{-3} in density and longer than the depth of focus in each case.

In Fig. 2 we indeed observe the same power scaling between the $f/7.5$ and $f/2$ cases in hydrogen. However, this is apparently fortuitous since there must be a difference in the plasma temperatures to account for the different acoustic shifts observed. To compare these results with theory, we rewrite Eq. (1) as

$$N=\alpha_{th}P_0=\left[1.06\times10^{-9}\,\frac{Ln_{17}Z}{\mu A\nu_9^2}\left(\frac{\omega_i}{\gamma_i}\right)\right]P_0, \tag{2}$$

where n_{17} is the electron density in units of 10^{17} cm^{-3}, Z is the average ion charge, μ is the ion mass in amu, A is the spot area, ν_9 is the ion acoustic frequency in GHz, and P_0 is the incident power in watts. The coefficient of P_0, α_{th}, is the theoretical slope of the power dependence curve (on a semi-log plot).

If we equate α_{th} to the experimentally observed slope, α_{ex}, and use the experimentally determined values of L, n_{17}, A, and ν_9, we find the value of γ_i/ω_i needed to make $\alpha_{ex}=\alpha_{th}$. Furthermore, if we assume that the Brillouin-driven ion acoustic wave is a natural mode of the plasma, then γ_i/ω_i is determined solely by the value of ZT_e/T_i through the dispersion relation[8]

$$2T_i/ZT_e=Z'[(\omega_i-i\gamma_i)/k_iV_{thi}], \tag{3}$$

where T_e and T_i are the plasma temperatures, $k_i\simeq 2k_0$ is the wavenumber of the ion acoustic wave (for backscatter), V_{thi} is the ion thermal velocity, and Z' is the derivative of the plasma dispersion function. We have assumed, legitimately, that $k_i^2\lambda_{De}^2\ll 1$, where λ_{De} is the Debye length.

Equations (1) and (2) are valid for $ZT_e/T_i=O(1)$ as long as ω_i and γ_i are taken to be consistent with Eq. (3).

For the $f/7.5$ focusing case, we find that $\alpha_{ex}=8.9\pm2.3\times10^{-6}$ W^{-1}. This agrees with α_{th} if $ZT_e/T_i=1.3\pm0.3$. The real part of the ion frequency is closely approximated by

$$\omega_i\simeq k_i[(ZkT_e+3kT_i)/M_i]^{1/2}, \tag{4}$$

and so we can find ZT_e from the measured frequency shift and the knowledge of ZT_e/T_i. This gives $T_e=12\pm2$ eV and $T_i=9\pm1$ eV ($Z=1$). Similarly, for the $f/2$ focusing case, we have $\alpha_{ex}=7.6\pm1.1\times10^{-8}$ W^{-1}, which gives $ZT_e/T_i=1.6\pm0.2$, $T_e=20\pm2$ eV and $T_i=13\pm1$ eV.

To check how well the convective theory has predicted our experimental results requires an independent check of these temperatures. We have one relation between T_e and T_i through the acoustic shift [Eq. (4)]. Another relation comes from the definition of the equilibration time, τ_{eq}, which is

$$\frac{dT_i}{dt}=\frac{T_e-T_i}{\tau_{eq}}.$$

If we assume that the electrons are quickly heated to T_e and maintained at that temperature for a time Δt, and that the ion temperature increases from $T_i=0$ at $\Delta t=0$, then[9]

$$T_e/T_i\simeq 1+\tau_{eq}/\Delta t, \tag{5}$$

where τ_{eq} is given, by

$$\tau_{eq}\simeq 3.14\,\frac{\mu T_e^{3/2}(ev)}{n_{17}Z^2\ln\Lambda}\ \text{nsec}. \tag{6}$$

We take Δt as the difference between the time at which the laser has finished ionizing along the depth of focus and the time of occurrence of Brillouin scattering, i.e., about 15 nsec. Combining Eqs. (5) and (6) and eliminating T_e/T_i with Eq. (4) yields an equation for T_e.

For the $f/7.5$ focusing case, this procedure gives $T_e\simeq 13.5$ and $T_i\simeq 9.1$, in good agreement with the inferred temperatures found earlier. For the $f/2$ case, we get $T_e\simeq 23$ eV and $T_i\simeq 12$ eV, again in good agreement.

We conclude that the experimental results do fit the convective theory of stimulated Brillouin scattering and that changing the focusing f number does not affect the produce I_0L in Eq. (1). However, the $f/2$ focusing resulted in a higher T_e and a larger T_e/T_i so that the product $\omega_i\gamma_i$ also remained approximately constant. Thus, there is no great difference in the observed Brillouin power dependence.

In the preceding discussion (and those to follow) we have assumed that the geometric factors L and A, and the plasma parameters n_{17}, Z, ν_9, and γ_i/ω_i do not vary significantly with incident power. In these experiments, L is generally determined by the depth of focus of the focusing lens and so is independent of P_0. Also, as discussed in the concluding section, we do not believe A is varying with P_0 in that there is no evidence for filamentation. In the hydrogen-target experiments, the pre-ionized gas becomes fully ionized along the depth of focus very early into the CO_2 laser pulse. The final density depends on how much time the plasma has to expand radially before the occurrence of Brillouin scattering. This time interval is found to be independent of P_0, and so n_{17} and Z in hydrogen are independent of P_0. The two remaining hydrogen plasma parameters and all four nitrogen plasma parameters may depend on P_0 through the power dependence of the electron temperature T_e. To get an idea of the strength of this dependence we have measured the acoustic shifts of the Brillouin backscatter with an incident power of about 150 MW, about half of our full input power. The measured acoustic shifts at half power agree with those at full power to within the approximately 20% uncertainty. From Eq. (4) we see that this implies that either ZT_e and T_i are constant or ZT_e and T_i change in opposite directions. Equations (5) and (6) imply, however, that T_i increases or decreases with T_e, so it must be that ZT_e and T_i are constant or are changing only weakly with incident power. For nearly constant T_e and ZT_e/T_i, we expect n_{17}, Z, and γ_i/ω_i to be nearly constant.

B. Z dependence

It was seen in Fig. 3 that the growth of Brillouin scattering with increasing power was much more rapid in nitrogen than in hydrogen. This can be understood by seeing how the exponentiation factor of Eq. (1) varies with mass and Z. We find that, for $ZT_e/3T_i \gg 1$,

$$N \propto I_0 L \frac{\omega_{pi}^2}{\omega_i^2}\frac{\omega_i}{\gamma_i} \propto \frac{I_0 L n_e}{T_e}\left(\frac{\exp(1+ZT_e/3T_i)}{(1+ZT_e/3T_i)}\right)^{3/2}.$$

In this limit, there is no dependence on ion mass, and the Brillouin scattering increases rapidly with ZT_e/T_i. For $ZT_e/T_i = O(1)$, N still increases with ZT_e/T_i, although not so rapidly.

From interferometry, we find that the density in nitrogen is about 1×10^{17} cm^{-3} and is uniform over the 1 cm depth of focus of the $f/7.5$ lens. We use Eq. (2) and follow the same procedure developed in the previous section to find that an experimental slope of $\alpha_{ex} = 2.4 \pm 0.7\times10^{-7}$ W^{-1} implies a temperature ratio of $ZT_e/T_i = 10.5 \pm 1.5$. In evaluating α_{th}, we assumed $Z=4$. From Eq. (4), for an acoustic shift of 9.5 GHz, we find that $ZT_e \simeq 290 \pm 8$ eV. Since the fourth ionization potential of nitrogen is about 77 eV, we see that $Z=4$ is a reasonable value to take. Thus, we find that $T_e \simeq 73 \pm 2$ eV and $T_i \simeq 28 \pm 3$ eV.

As a cross check, we can use the acoustic shift plus equilibration time formulism to find that, for $Z=4$ and $\Delta t = 25$ nsec, T_e is approximately 74 eV and T_i is approximately 25 eV. This agrees quite well with the values obtained from the slope. Finally, to compare with hydrogen, we see that the number of e foldings of Brillouin scatter above noise when P_0 is 100 MW (where the reflectivity in nitrogen begins to saturate) is $N = \alpha_{ex}P_0 = 24 \pm 7$ in nitrogen and $N = 8.9 \pm 2.3$ in hydrogen. Thus, the Brillouin growth in nitrogen is larger by a factor of 3×10^6 than in hydrogen because of the increased ZT_e/T_i and, consequently, the reduced ion wave damping in the nitrogen plasma.

Although there is much more Brillouin growth in nitrogen than in hydrogen, the reflectivities at 100 MW differ by only a factor 10^2. Apparently, the noise level from which Brillouin grows in hydrogen is approximately 10^4 times the noise level in nitrogen. We have previously reported noise levels of 10^3–10^5 times the thermal Thomson scattering level in hydrogen.[2] This was attributed to scattering from ion acoustic turbulence in an ionization front. The presence of this ionization is characteristic of the laser heating and ionization of our pre-ionized hydrogen gas target.

In the nitrogen target, however, we do not observe an ionization front during the laser heating, possibly because the low ionization potential of nitrogen does not allow the existence of a suitable temperature jump necessary for an ionization front. Without the ionization front the Brillouin scatter from nitrogen may be growing from the thermal Thomson scattering level. The inferred noise level is roughly $P_n/P_0 = 10^{-15}$–10^{-9}. This compares with the calculated thermal Thomson scattering level of approximately 10^{-11} calculated for the nitrogen plasma parameters of $n_e = 1\times10^{17}$ cm^{-3}, $Z=4$, $T_e = 73$ eV, and $T_i = 28$ eV. Thus, the Brillouin scatter in nitrogen could be growing from the thermal Thomson scattering level.

TABLE II. Brillouin reflectivities at the onset of saturation and at full power with the various f number and gas combinations.

Gas (f number)	P_0 at knee (MW)	R at knee (%)	Max. P_0 (MW)	Max. R (%)
$H_2(f/7.5)$	190	3.0	340	8.5
$H_2(f/2)$	190	0.7	350	1.6
$N_2(f/7.5)$	100	2.5	330	8.5

C. Saturation levels

The reflectivities at the onset of saturation, i.e., at the "knee" of the growth curve, and the maximum reflectivities at maximum input power are summarized in Table II. If we assume that the reflectivity is limited solely by the maximum amplitude of the ion acoustic wave, then we can estimate the saturated level of the ion acoustic density fluctuations.

If the ion wave amplitude is uniform over the length L, then the reflectivity is given by the usual Bragg scattering formula as $ZT_e/3T_i = O(1)$,

$$R = \left(\frac{\pi}{2}\frac{n_0}{n_c}\frac{L}{\lambda_0}\frac{\tilde{n}}{n_0}\right)^2, \tag{7}$$

where $\tilde{n}/n_0$ is the density fluctuation level normalized to the electron density, and n_c is the critical density for light of vacuum wavelength λ_0. However, for our experimental conditions, the stimulated Brillouin scattering instability is in the convective regime,[10] which means that the ion wave amplitude varies greatly over the length L. In the strong damping case, $ZT_e/3T_i = O(1)$, the ion wave amplitude is related locally to the incident and reflected wave fields by[11]

$$\tilde{n}(x)/n_0 = (Zk_i^2 r_0/4M_i\gamma_i\omega_i)A_s(x)A_0(x), \tag{8}$$

where M_i is the ion mass, $A_s(x)$ is the local vector potential of the scattered wave, and $A_0(x)$ is that of the incident wave. We neglect pump depletion and rewrite Eq. (8) as

$$\frac{\tilde{n}(x)}{n_0} = \frac{4\pi r_0}{mc^2\omega_0}\frac{\omega_{pi}^2}{\omega_i\gamma_i}\left(\frac{1}{\pi}\frac{n_c}{n_0}\frac{\lambda_0}{L}\right)I_0 L\frac{A_s(x)}{A_0} = \frac{N}{\beta L}\frac{A_s(x)}{A_0}, \tag{9}$$

where we have used Eq. (1) for N, set $k_i = 2k_0$, and defined β as

$$\beta \equiv (n_0/n_c)(\pi/\lambda_0). \tag{10}$$

Let us choose positive x in the incident k_0 direction and define the interaction region as $0 \le x \le L$. Since we have a convective instability, we know that the scattered power $P_s(x)$ grows from the noise level, $P_n \equiv P_s(L)$, at $x=L$ to the final detected level, $P_s \equiv P_s(0) = P_n e^N$, at $x=0$; i.e.,

$$P_s(x) = P_n \exp[N(1-x/L)], \quad 0 \le x \le L.$$

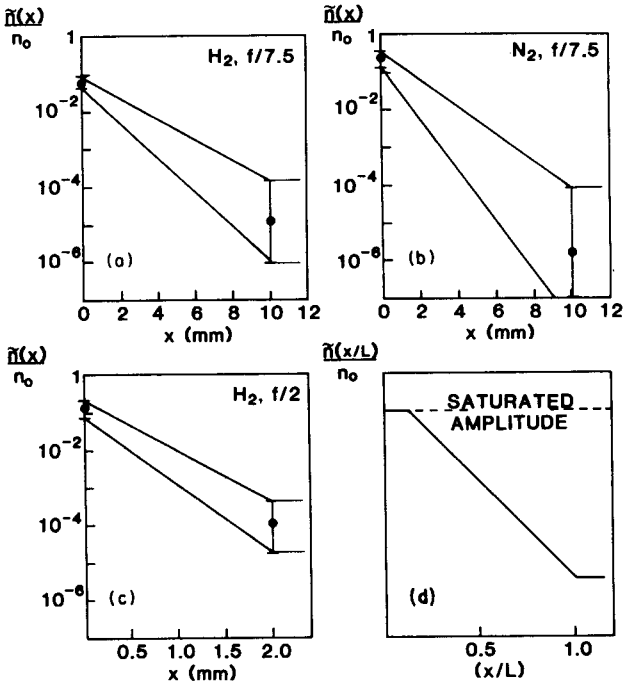

FIG. 5. Ion acoustic wave amplitude $n(x)/n_0$ vs x for the cases: (a) H_2, $f/7.5$; (b) N_2, $f/7.5$; (c) H_2, $f/2$, all at saturation. (d) Schematic log plot of n/n_0 showing a possible cause of the increasing reflectivity beyond "saturation."

In terms of amplitudes, we have

$$A_s(x)/A_0 = (A_n/A_0)\exp[\tfrac{1}{2}N(1-x/L)]$$
$$= (P_n/P_s)^{1/2}(P_s/P_0)^{1/2}\exp[\tfrac{1}{2}N(1-x/L)].$$

But, $P_s/P_n = e^N$ and $P_s/P_0 = R$ so that Eq. (9) becomes

$$\tilde{n}(x)/n_0 = (NR^{1/2}/\beta L)\exp(-Nx/2L), \quad 0 \le x \le L. \tag{11}$$

The maximum value of $\tilde{n}(x)/n_0$ occurs at $x=0$ and is a factor of $N/2$ larger than predicted by Eq. (7).

The quantities N, R, β, and L are all determined experimentally. Plots of $\tilde{n}(x)/n_0$ vs x are shown in Figs. 5(a), (b), and (c) for various f number and Z combinations. The error bars at $x=0$ represent the uncertainty in $NR^{1/2}/\beta L$, while the error bars at $x=L$ reflect the uncertainty in N through $\exp(N/2)$. These plots represent the spatial variation of $\tilde{n}(x)/n_0$ at the knee of the growth curves, at the onset of saturation. Therefore, we shall take the amplitude at $x=0$ as the saturated or maximum ion acoustic wave amplitude. The slow rise in reflectivity beyond the knee in Figs. 2 and 3 could be due to a flattening of $\tilde{n}(x)/n_0$ near $x=0$ as illustrated in Fig. 5(d). In fact, the saturated value of $\tilde{n}/n_0$ need only extend a fraction of $L/10$ to account for the increased reflectivity at full input.

We now consider some likely ion wave saturation mechanisms. These are; (i) ion trapping,[12,13] (ii) ion heating,[11] and (iii) harmonic generation/wave breaking.[12] Ion heating would increase the damping rate of the ion acoustic wave and hence could limit its amplitude; it occurs when the ions extract energy, via Landau damping, from the ion acoustic wave. The energy of the ion acoustic wave is extracted from the pump plus reflected wave and so the ion heating rate is a function of the reflectivity. For our low reflectivities (<10%) and short Brillouin time scales (<5 nsec), there is not enough time for significant ion heating.[11]

Harmonic generation and wave breaking in low amplitude, free-traveling ion acoustic waves both imply steepened wave crests and eventual collapse of the wave for amplitudes above some critical value. This is supposed to happen when $\tilde{n}/n_0 \sim k_i^2\lambda_{D_e}^2 \simeq 0.5\%$ in hydrogen and approximately 6% in nitrogen. This is much lower than the inferred $\tilde{n}/n_0$ of 6–13% in hydrogen and approximately 25% in nitrogen. However, the ion acoustic waves in stimulated Brillouin scattering are not free-traveling but are pumped locally at a fixed ω_i and k_i as they propagate, perhaps resulting in a lower harmonic content and, therefore, less tendency to break.

Ion trapping is a more likely saturation mechanism. The time for a resonant ion to become trapped, τ_t, is related to the bounce frequency of the resonant ion and is given by[14]

$$\tau_t \simeq \sqrt{2}\,\pi(M/ZeEk_i)^{1/2}, \tag{12}$$

where E is the electric field of the ion wave. For our inferred maximum ion wave amplitudes, this gives typically $\tau_t = 200$–400 psec, which is much less than the duration of the Brillouin backscatter signal. Ion trapping is supposed to limit the ion wave amplitude to[12]

$$\frac{\tilde{n}}{n_0} \simeq \frac{1}{2}\left[\left(1+\frac{3T_i}{ZT_e}\right)^{1/2} - \left(\frac{3T_i}{ZT_e}\right)^{1/2}\right]^2. \tag{13}$$

Figure 6 shows a plot of this saturation amplitude along with the experimentally inferred points for the three cases. The two low-intensity, $f/7.5$ points do intercept this curve, but the high intensity $f/2$ point is well above it. In considering the $f/2$ case, we have neglected some possible effects; namely, three-dimensional effects due to the relatively large range of angles involved in focusing the beam, and light pressure effects

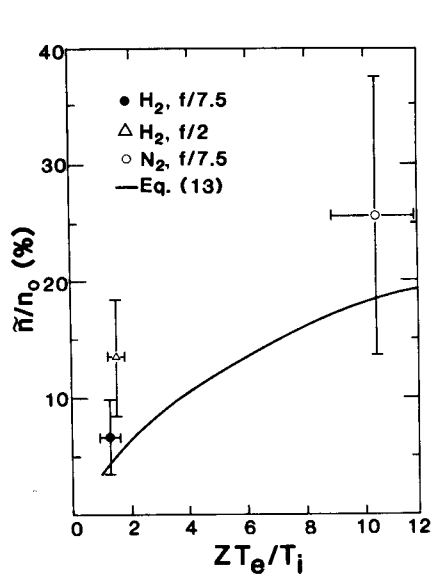

FIG. 6. Inferred ion acoustic wave saturated amplitudes vs ZT_e/T_i for: H_2, $f/7.5$ (●); H_2, $f/2$ (△); and N_2, $f/7.5$ (○). Solid line is the theoretical prediction of the saturated wave amplitude.

due to $V_0^2/V_{th\,e}^2 > 1$, where V_0 is the electron quiver velocity in the incident laser field and $V_{th\,e}$ is the electron thermal velocity. To lowest order, we would not expect the three-dimensional effects to be important because, in the ideal case, the laser light wave is essentially a plane wave along the depth of the focus regardless of f, because the ratio of depth of focus to spot diameter is independent of f number. Thus, in a gas target experiment, three-dimensional effects are not necessarily more important for smaller f numbers, although the possibility remains open.[15] Light pressure effects such as self-focusing and filamentation, if present, would certainly alter our interpretation of the data but, as discussed in the concluding section of this paper, are not believed to be present.

D. Light ion impurity

In comparing the growth curves [Fig. 4(a)] in pure nitrogen (N_2) and nitrogen plus 8% hydrogen ($N_2 + H_2$), three observations can be made: (1) the reflectivity in $N_2 + H_2$ is saturated and is nearly 20 times below that in N_2; (2) the slope of the $N_2 + H_2$ curve appears to be much less than that of the N_2 curve; and (3) if observation (2) is correct, then the noise level from which the Brillouin scattering grows is much higher in the $N_2 + H_2$ case.

Drawing lines through the three lowest power points of the $N_2 + H_2$ growth curve allows us to estimate the slope at $\alpha_{ex} \simeq 2.9 \pm 1.8 \times 10^{-8}$ W^{-1}. This compares with $\alpha_{ex} \simeq 2.4 \pm 0.7 \times 10^{-7}$ W^{-1} in pure nitrogen. From Eq. (2) we see that $\alpha_{th} \propto n_e(\omega_i \gamma_i)^{-1}$, so that the most likely cause of a 5 to 27 times decrease in α_{ex} is a corresponding increase in γ_i. If we write Eq. (3) for two ion species and expand in large ZT_e/T_i, we find that γ_i should increase about three times with an 8% proton impurity, all else being constant; but all else is not constant. The observed acoustic shift in $N_2 + H_2$ is about 8 GHz compared with about 9.5 GHz in pure nitrogen, which means that the phase velocity of the ion wave is reduced (through lower T_e), thus further increasing the Landau damping rate.

The scattered power in the $N_2 + H_2$ case is very irreproducible at input powers below about 60 MW, thus making it impossible to verify whether or not the noise level, P_n/P_0, is really 10^{-3} to 10^{-5}, as implied from the growth curve.

Finally, we note that the reduced saturated reflectivity [Figs. 4(a) and (b)] is qualitatively consistent with the idea of trapping in that adding the light ions, which travel closer to the phase velocity, causes trapping to begin at smaller amplitudes.

V. CONCLUSION

In this paper we have presented some experimental observations on the focusing f number and target material dependence of stimulated Brillouin scattering. We find that reducing the f number of the focusing lens has little effect on the power dependence of the stimulated Brillouin scattering because the increased intensity is offset by the reduced depth of focus. However, the inferred saturation level of the ion acoustic wave seems to be higher with the lower f number. This may be due to three-dimensional effects or to higher light pressure ($V_0^2/V_{th\,e}^2 > 1$) effects. The stimulated Brillouin scattering growth in nitrogen is found to be much more severe than in hydrogen because the nitrogen plasma has a higher ZT_e/T_i, resulting in lower damping of the ion acoustic wave. The inferred saturated amplitudes of the ion acoustic waves are consistent with ion trapping as a saturation mechanism. We also find that a small amount ($\simeq$6%) of hydrogen impurity added to a nitrogen plasma greatly reduces the level of stimulated Brillouin scattering, as expected; and there is some indication that the noise level is greatly enhanced with the impurity. Finally, when the laser is operating on three lines, we find that the stimulated Brillouin scattering is reduced as if one line were acting independently of the other two, again as expected.

These conclusions assume the absence of any filamentation in the CO_2 laser beam. While filamentation under these experimental conditions is theoretically possible, a sensitive photographic technique used to find filamentation under different conditions[16] revealed no evidence for filamentation for these conditions.

ACKNOWLEDGMENT

This work was supported by the Los Alamos Scientific Laboratory, Work Order 4-XPO-1033P-1.

[1] J. F. Drake, P. K. Kaw, Y. C. Lee, G. Schmidt, C. S. Liu, and M. N. Rosenbluth, Phys. Fluids **17**, 778 (1974).
[2] M. J. Herbst, C. E. Clayton, and F. F. Chen, Phys. Rev. Lett. **43**, 1591 (1979).
[3] F. J. Mayer, G. E. Busch, C. M. Kinzer, and K. G. Estabrook, Phys. Rev. Lett. **44**, 1498 (1980).
[4] A. Ng, L. Pitt, D. Salzmann, and A. A. Offenberger, Phys. Rev. Lett. **42**, 307 (1979).
[5] M. J. Herbst, C. E. Clayton, W. A. Peebles, and F. F. Chen, Phys. Fluids **23**, 1319 (1980).
[6] M. Q. Tran and S. Coquerand, Phys. Rev. A **14**, 2301 (1976).
[7] J. J. Thomson, Nucl. Fusion **15**, 237 (1975).
[8] B. D. Fried and S. D. Conte, *The Plasma Dispersion Function* (Academic, New York, 1961).
[9] M. J. Herbst, C. E. Clayton, and F. F. Chen, J. Appl. Phys. **51**, 4080 (1980).
[10] D. W. Forslund, J. M. Kindel, and E. L. Lindman, Phys. Fluids **18**, 1002 (1975).
[11] W. L. Kruer, Phys. Fluids **23**, 1273 (1980).
[12] J. M. Dawson, W. L. Kruer, and B. Rosen, in *Dynamics of Ionized Gases*, edited by M. Lighthill, I. Imai, and H. Sato, (University of Tokyo Press, Tokyo, 1973), p. 47.
[13] H. Ikezi, K. Schwarzenegger, A. L. Simons, Y. Ohsawa, and T. Kamimura, Phys. Fluids **21**, 239 (1978).
[14] J. M. Dawson, Phys. Fluids **4**, 869 (1961).
[15] Z. A. Pietrzyk and T. N. Carlstrom, Appl. Phys. Lett. **35**, 681 (1979).
[16] C. Joshi, C. E. Clayton, A. Yasuda, and F. F. Chen, J. Appl. Phys. (to be published, January 1982).